Electronic structure of Co^{2+} ions in anatase Co:TiO_2 in relation to heterogeneity and structural defects

Y. J. Lee, M. P. de Jong, and W. G. van der Wiel
NanoElectronics Group, MESA+ Institute for Nanotechnology, University of Twente, 7500 AE Enschede, The Netherlands
(Received 7 December 2010; published 5 April 2011)

We have studied the electronic structure of Co ions in semiconducting anatase Co:TiO_2(1.4 at.% Co) with x-ray-absorption spectroscopy. The density of structural defects is varied by (i) the oxygen vacancy concentration depending on the oxygen background pressure during growth, and (ii) the film thickness. The Co $L_{2,3}$-edge spectra, which are characteristic of Co^{2+} ($3d^7$) ions, show particularly pronounced ligand-to-metal charge-transfer (CT) satellites for the thickest oxygen-poor films, which also exhibit the highest structural defect density. With charge-transfer multiplet calculations, the CT satellites are modeled by configuration interaction, originating from hybridization between Co 3*d*- and ligand states. This hybridization adds to the complex interplay between Co heterogeneity, defects, and electronic and magnetic properties in Co:TiO_2.

DOI: 10.1103/PhysRevB.83.134404 PACS number(s): 78.70.Dm, 75.50.Pp, 75.47.Lx

I. INTRODUCTION

Dilute magnetic semiconductors (DMSs) are of great interest for the realization of practical, semiconductor-based spintronic applications. A DMS, containing a dilute concentration of magnetic ions imbedded in a semiconductor host lattice, is characterized by carrier mediated exchange interactions between the magnetic ions. In such systems, the magnetic properties can be controlled by tuning the carrier concentration (e.g., via electrical gating), and the carriers are spin polarized in the ferromagnetic state. However, the low ferromagnetic ordering temperatures attainable so far preclude practical applications. Therefore the theoretical prediction by Dietl *et al.*[1] of room-temperature ferromagnetism in transition-metal doped wide band-gap oxides and nitrides has initiated a strong effort focused on the development of room-temperature DMS systems based on such materials. In particular, cobalt-doped TiO_2 (Co:TiO_2) has received much attention, following the initial observation of room-temperature ferromagnetism by Matsumoto *et al.*[2]

Up to now, many reports on Co:TiO_2 have been published that demonstrate not only room-temperature ferromagnetism, but also anomalous Hall effects (AHEs) in both rutile and anatase Co:TiO_2,[3–7] magneto-optical effects,[7,8] and tunneling magnetoresistance.[9] However, in spite of these encouraging results, there is also a large amount of evidence that points toward extrinsic sources of ferromagnetism (see, e.g., Ref. 10, and references therein), i.e., ferromagnetic ordering not arising from carrier mediated exchange. To date, strong controversy persists about the origin of ferromagnetism, and related effects like the anomalous Hall effect, mainly due to conflicting results and doubts about the validity of said results. The complexity of the issue is partially due to the strong impact of growth conditions and thermal treatment on structural, electronic, and magnetic properties. The thin films, and in particular the Co dopants, are not in thermodynamic equilibrium, stimulating heterogeneity via precipitation of parasitic phases, spinodal decomposition, etc. Even in the absence of such spurious effects, however, the exchange interactions between ordered spins might be mediated by complex electronic defects,[11] involving ensembles of, e.g., magnetic dopant ions in substitution or interstitial positions, oxygen vacancies, and adjacent ions from the host cation sublattice. Moreover, an important role in the formation of such complex defects is ascribed to surfaces and interfaces of the thin films.

In a previous work,[12] we addressed the heterogeneity of Co (metallic Co clusters in addition to ionic Co^{2+}) in relation to the magnetic properties of both ferromagnetic and paramagnetic Co:TiO_2 thin films prepared by pulsed laser deposition (PLD) at different oxygen background pressures. Using x-ray-absorption spectroscopy (XAS), x-ray magnetic circular dichroism (XMCD), and (energy filtered) transmission electron microscopy (EF-TEM), we showed that the Co distribution is heterogeneous for Co:TiO_2 films grown under oxygen-rich (resulting in paramagnetic behavior) as well as oxygen-poor conditions (yielding ferromagnetic properties), and more so for the latter. We observed substitutional Co^{2+} using XAS (i.e., Co^{2+} in a quasioctahedral bonding environment), which might be correlated with earlier observations of impurity band conduction,[13] whereas XMCD measurements and EF-TEM showed the presence of metallic Co, which contributes to the ferromagnetism and AHE.[6] In this work, we perform a detailed XAS analysis of the electronic properties of ionic cobalt (Co^{2+}) in Co:TiO_2(1.4 at.% Co) on $SrTiO_3$, and provide evidence for Co heterogeneity other than the previously discussed metallic phases. The observed differences in the XAS spectra can be correlated with a variation of the abundance of structural defects in the samples, which we control via (i) the oxygen pressure during growth, and (ii) the film thickness.

II. EXPERIMENT

Epitaxial thin films of anatase Co:TiO_2 (1.4 at.%) were grown by pulsed laser deposition on TiO_2-terminated (100) $SrTiO_3$ substrates under oxygen-rich (10^{-3} mbar) and oxygen-poor (9×10^{-5}mbar) conditions (hereafter referred to simply as "oxygen-rich" and "oxygen-poor" samples). $SrTiO_3$ substrates were chemically treated and annealed at 950°C to obtain a TiO_2 termination. Ablation of a $Co_xTi_{1-x}O_2$ ($x = 0.014$) target

 ©2011 American Physical Society

was carried out using a KrF excimer ($\lambda = 248$ nm) laser with a fluence of 1.8 J/cm^2 at a rate of 5 Hz. The substrate temperature during growth of the films was fixed at 550°C. X-ray-absorption spectroscopy measurements were performed at beam line I1011 of MAX-lab in Lund, Sweden. All spectra were measured at room temperature in total electron yield mode, with a probing depth of about 10 nm.[14] The photon flux was monitored using the electron yield from a gold grid. The photon linewidth was set to 120 meV for Co L-edge measurements, while the polarization was fixed in the horizontal plane. Atomic force microscopy (AFM) and energy filtered transmission electron microscopy was carried out to investigate structural defect formation in the films.

III. COMPUTATIONAL DETAILS

Charge-transfer multiplet (CTM) calculations were performed using code developed by Thole and co-workers, based on Cowan's atomic multiplet code and Butler's group-theoretical code.[15] Due to the strong Coulomb interaction between the $2p$ core holes and the $3d$ valence electrons, the core-excited states remain largely localized on the Co ions, such that the $L_{2,3}$-edge XAS spectra can be interpreted in terms of atomic multiplet structure. Recently, *ab initio* configuration interaction methods based on relativistic density-functional theory have been developed by the Tanaka group (see, e.g., Ref. 16), which employ molecular orbitals as basis functions without adjustable parameters. Here, we have chosen for the computationally much less costly semiempirical CTM calculations, which have been shown to give a good description of the XAS spectra of transition-metal compounds featuring charge-transfer effects. Moreover, *ab initio* calculations would be difficult to perform for systems comprising considerable structural (and chemical) heterogeneity and defects. In the semiempirical approach used here, the interaction between Co ions and the neighboring oxygen atoms is taken into account in a simple way by (i) lowering the ground-state symmetry and the introduction of a crystal field, and (ii) modeling of hybridization effects involving metal $3d$ states and ligand bands via configuration interaction. We use an octahedral crystal field, with the $10Dq$ parameter corresponding to the splitting between the t_{2g} and e_g states set to 1.1 eV in both the initial and final state. As has been shown previously using ligand field multiplet calculations,[12] this gives a good description of the XAS spectral shape of the substitutional Co^{2+} ions in our Co:TiO_2 thin films, which closely resembles that of the Co L edge of CoO. The latter contains Co^{2+} ions in an octahedral crystal field with a $10Dq$ parameter of 1.05 eV.[17]

The Hartree-Fock Slater integrals were scaled to 75% of their atomic values, as in our previous work,[12] to account for intra-atomic configuration interaction and, to a lesser extent, electron delocalization effects associated with covalency.[15,18] To allow for a straightforward comparison to experiments, the calculations are convoluted with Lorentzian and Gaussian functions to account for, respectively, lifetime broadening and experimental resolution. The Lorentzian lifetime width is set to 0.2 and 0.4 eV for the L_3 and L_2 edges, respectively, while the Gaussian width is fixed at the experimental photon linewidth of 120 meV.

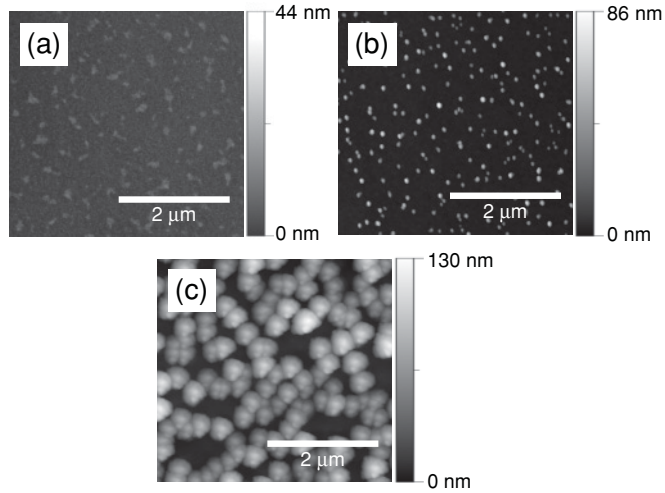

FIG. 1. AFM images of a 45-nm-thick oxygen-rich sample with 1.4 nm rms roughness (a), a 45-nm-thick oxygen-poor sample with 4.5 nm rms roughness (b), and 160-nm-thick oxygen-poor sample with 25.5 nm rms roughness (c).

IV. RESULTS AND DISCUSSION

We start with a discussion of the structural properties of the Co:TiO2 thin films in relation to the oxygen pressure during growth and the film thickness. Films prepared under oxygen-rich conditions, i.e., 10^{-3} mbar oxygen during growth, are characterized by a high structural quality. These films exhibit relatively flat surfaces [see Fig. 1(a)] showing an AFM image of a 45-nm-thick oxygen-rich film with root-mean-square (rms) roughness of 1.4 nm), a well-defined epitaxial relation with the STO substrate, only very few parasitic phases such as outgrowths and Co-rich clusters, and sharp Co $L_{2,3}$-edge features.[12] In contrast, oxygen-poor samples show an increased roughness [4.5 nm rms as obtained from AFM analysis of a 45-nm-thick oxygen-poor film shown in Fig. 1(b)], exhibit significantly stronger Co heterogeneity,[12] and develop an increasing areal density of outgrowths with increasing thickness [see Figs. 1(b) and 1(c)]. In particular, the 160-nm-thick oxygen–poor sample features significant outgrowths of about 90 nm in height [see Fig. 1(c)]. These outgrowths can be assigned to rutile polycrystallites, as is evident from a comparison of the Ti L-edge XAS spectra of 10- and 160-nm oxygen-poor Co:TiO_2 films (Fig. 2). The XAS spectrum of the 160-nm film, having a large areal density of outgrowths, features a clear increase of the shoulder at about 461 eV photon energy. This shoulder is indicative of the presence of parasitic rutile phases, as is well known from the literature on Ti L-edge XAS of anatase and rutile.[19] Rutile, being the more stable polymorph, is well known to form on anatase films when nucleation sites, such as dislocations and grain boundaries, are present.[20,21] The inclusion of oxygen vacancies, which is necessary for obtaining room-temperature ferromagnetism, thus stimulates the formation of lattice defects, which become more abundant as the thickness increases and the strain relaxes via the formation of, e.g., dislocations. The presence of the Co^{2+} ions, which have a significantly larger ionic radius than Ti^{4+},[22] is also thought to play a role in the formation of (extended) defects, due to the lack of

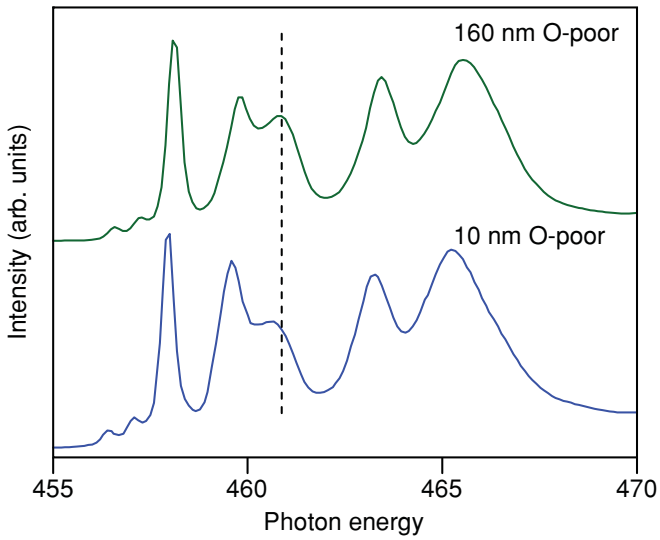

FIG. 2. (Color online) Ti *L*-edge XAS spectra of 10-nm- and 160-nm-thick oxygen-poor films. The dashed line indicates the position of the shoulder that is indicative of parasitic rutile phases.

thermodynamic equilibrium introduced by these species. It should be pointed out in this respect that a higher amount of oxygen vacancies in the host lattice facilitates the diffusion, and thus segregation, of Co^{2+}. Indeed, the formation of rutile outgrowths and Co segregation appear to be correlated.[12,23] This is illustrated in Fig. 3, showing Ti and Co maps obtained by EF-TEM of a 160-nm oxygen-poor film. We performed a large number of similar measurements, from which it can be concluded that Co clusters are found underneath nearly every outgrowth. Previously, we have shown that Co segregation and the associated formation of metallic clusters has a profound impact on the magnetic properties,[12] including the anomalous Hall effect,[23] of Co:TiO_2 films. An interesting question, which we address now, is whether there is any impact of the formation of defects/outgrowths on the electronic properties of Co *ions* in these films. After all, the chemical bonding environment of Co ions might be expected to be different in heavily defected regions.

A comparison of the spectral features of the Co $L_{2,3}$-edge XAS spectra of Co:TiO_2 thin films, all with a cobalt concentration of 1.4 at.%, with a varying defect density, is shown in Fig. 4. Three different cases are considered: a

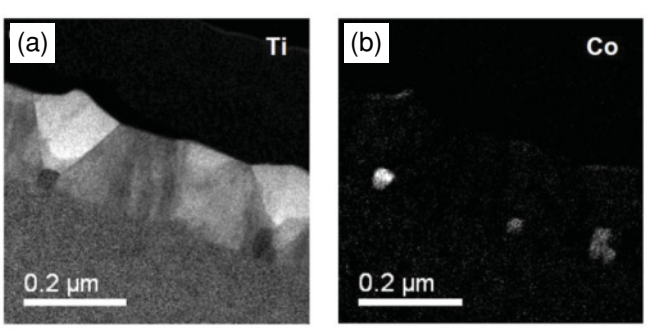

FIG. 3. EF-TEM images of a 160-nm oxygen-poor Co:TiO_2 film. The images represent concentration maps (in white) of Ti (a), and Co (b).

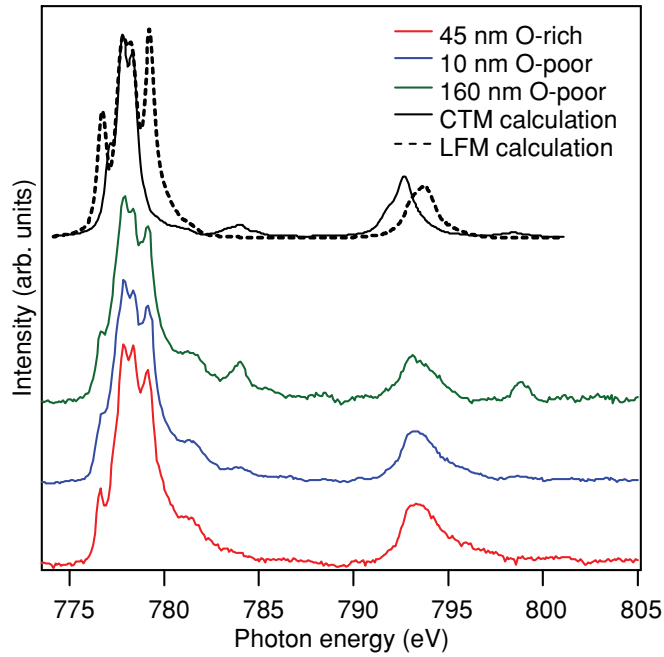

FIG. 4. (Color online) Co *L*-edge XAS spectra (normalized to the same peak height) of three different Co:TiO_2 thin films: a 45-nm oxygen-rich film (red, bottom), a 10-nm oxygen-poor film (blue, second from bottom), and a 160-nm oxygen-poor film (green, third from bottom). Simulated spectra obtained from ligand field multiplet LFM (black dashed line, top) and CTM (black solid line, top) calculations are also shown.

45-nm oxygen-rich film, and 10-nm- as well as 160-nm-thick oxygen-poor films. There are two clear differences in the XAS spectra for oxygen-rich versus oxygen-poor samples. The first difference, a suppression/smearing of the multiplet structure in oxygen-poor films, was already discussed by us previously,[12] and can be attributed in part to an increased amount of metallic Co as compared to that in oxygen–rich films. The second difference is the observation of satellite features, similar to those previously observed in related systems,[24,25] about 7 eV above the L_2 and L_3 edges, in the XAS spectra of the oxygen-poor samples. Lussier *et al.* reported Co *L*-edge data of both rutile and anatase Co:TiO_2 (Co concentration 7 at.%) that showed a similar feature for rutile samples, but not for anatase.[24] Although the authors pointed out the difference, the origin of the peak was not explained. Liu *et al.* also observed a satellite feature in Co *L*-edge XAS spectra of Co:ZnO (5 at.% Co) and Co/Al:ZnO (5 at.% Co, 1 at.% Al).[25] The authors did not include a calculation, but did attribute the feature to ligand-to-metal charge transfer (CT), which they considered to be dependent on the extent of delocalization of donor defect states (i.e., oxygen vacancies and Al ions). As we will show below using CTM calculations, the satellite peaks can indeed be understood in terms of CT. In our study, there appears to be a strong relation between the intensity of the satellite peaks in the Co *L*-edge XAS spectra and the defect density. The additional peaks are absent, or at least too weak to be discernable, for the oxygen-rich film exhibiting high structural quality, while the intensity of the satellites is clearly highest for the 160-nm-thick oxygen-poor film, which is characterized by a large abundance of defected regions (outgrowths). We

confirmed these findings for a range of oxygen-poor samples prepared under identical conditions with thickness 10, 20, 40, and 160 nm, and consistently found the strongest satellite features for the thickest films.

We now turn to the CTM calculations, in which the ground-state and final-state configurations were modeled as a mixture of $3d^7$ and $3d^8\underline{L}$. We adjusted the energy difference between these different configurations to obtain a good description of the experimental spectra, in particular the relative excitation energy and intensity of the satellite peaks. The calculated spectrum shown was obtained by setting the ground-state energy difference between the $3d^7$ and $3d^8\underline{L}$ configurations to $\Delta = 1.5$ eV. The energy difference in the final state, i.e., for the configurations $5p^5 3d^8$ and $2p^5 3d^9\underline{L}$, was set to $\Delta' = \Delta + U_{pd} + U_{dd} = -0.5$ eV. It is thus reasonably assumed that the core-hole potential U_{pd} is 2 eV larger than the on-site Hubbard d-d repulsion energy U_{dd} (values for $U_{pd} - U_{dd}$ between 1 and 2 eV are routinely used in the literature; see, e.g., Ref. 26). The transfer integrals, which determine the effective hopping bandwidth that couples the two electronic configurations, were kept fixed at $T_{eg} = 2$ and $T_{t2g} = 1$ eV. These are typical values applied for transition-metal oxides featuring σ bonding, where larger values are expected for e_g orbitals pointing toward the oxygen ligands. The crystal-field parameter $10Dq$ was set to 1.1 eV in both the initial and final state, similar to previously performed ligand field multiplet (LFM) calculations.[12] Using these parameters, we are able to reproduce a CT satellite feature in the calculations with a fairly strong intensity, at the same excitation energy relative to the main $L_{2,3}$ edges where it appears in the experimental data. In this respect, the CTM calculations seem to describe the observations well. It is clear, however, that a description in which all Co ions are in a mixed $3d^7$ and $3d^8\underline{L}$ state falls short, since the Co L edge, apart from the satellite, strongly resembles that of a pure $3d^7$ configuration for all samples. The calculated spectrum of the mixed $3d^7$ and $3d^8\underline{L}$ bears strong $2d^8$ character with a "contracted" multiplet structure, similar to other $3d$ transition-metal compounds featuring small values of Δ.[26,27] This observation yet again points towards Co heterogeneity, in which some Co ions are strongly coupled to donor defect states in the gap that are energetically close to the $3d$ states, while others remain essentially unperturbed. Given that the samples indeed contain various different phases (e.g., Co-rich clusters, rutile outgrowths), this is perhaps not surprising. The XAS spectra can thus best be interpreted as a sum of various different contributions, related to a Co^{2+} $3d^7$ configuration, Co^{2+} with a mixed $3d^7$ and $3d^8\underline{L}$ configuration, and metallic Co (evidence for the latter can be found in Ref. 12).

We finally address an exceptional case, namely that of a 2-nm Co:TiO_2 film, deposited onto a layer stack comprising STO (substrate)/$La_{0.7}Sr_{0.3}MnO_3$ (LSMO 8.5 nm)/STO (3.1 nm), similar to structures we used in our studies of magnetic tunnel junctions (MTJs) containing ultrathin Co:TiO_2 layers.[28] Since the film thickness is merely 2 nm, corresponding to the height of about two anatase unit cells (c axis 0.915 nm), such films exhibit considerable strain, as can be deduced from a comparison of the (bulk) lattice parameters: $a_{\mathrm{LSMO}} = 0.3873$ nm, $a_{\mathrm{STO}} = 0.3905$ nm, $a_{\mathrm{anatase}} = 0.3785$ nm. This leads to a distortion of the TiO_6 octahedra away from their equilibrium geometry, which gives rise to a slightly different quasioctahedral bonding environment for substitutional Co ions. Indeed, the XAS multiplet structure of the 2-nm Co:TiO_2 film confirms this (see Fig. 5). The multiplet splitting is somewhat reduced as compared to that of thicker films, which can be modeled in the most straightforward way via a reduction of the cubic crystal-field strength $10Dq$ (see Fig. 5). This is consistent with tensile strain in the Co:TiO_2 film, and a correspondingly larger unit-cell volume, resulting from the different lattice parameters of the materials in the stack.

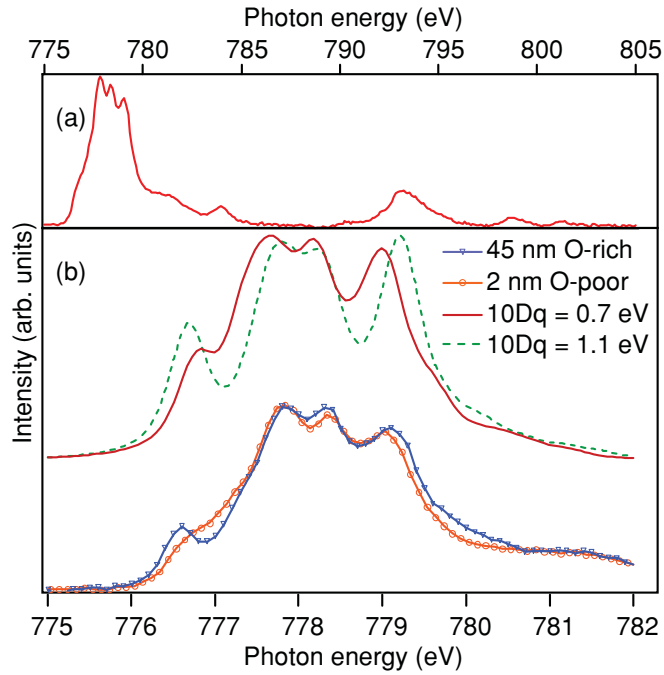

FIG. 5. (Color online) (a) Co L-edge spectrum of a 2-nm oxygen-poor Co:TiO_2 film in a MTJ stack (see text), (b) Co L_3-edge spectra of the same 2-nm Co:TiO_2 film (orange circles) and a 45-nm oxygen-rich Co:TiO_2 film (blue triangles), accompanied by calculated spectra using LFM calculations with $10Dq$ set to 1.1 eV (green dashed line) and 0.7 eV (red solid line).

Also this sample, comprising a 2-nm Co:TiO_2 film, exhibits clear CT-satellite peaks at the Co L edges. At first this may seem surprising in light of the discussion above, where the increased intensity of the CT feature was correlated with a higher density of defect gap states in thick (e.g., 160 nm) films. For a 2-nm film, a scenario involving stronger CT peaks, as compared to 10- or 20-nm-thick films, from a larger density of donor defect states is not realistic. Instead, the CT features could possibly arise from interfacial electronic states involving Co($3d$) orbitals, and STO and/or TiO_2 interface states. Indeed, it might be expected that Co ions prefer interfacial positions, e.g., substituting Ti^{4+} ions at the interface, due to the large mismatch between the Co^{2+} and Ti^{4+} ionic radii.

V. SUMMARY AND CONCLUSIONS

We have presented Co L-edge XAS data of Co:TiO_2 thin films that exhibit distinct satellite peaks at about 7 eV above the main x-ray-absorption edges. We model these features using charge-transfer multiplet calculations, and find a fairly good agreement for a mixed $3d^7$ and $3d^8\underline{L}$ electronic configuration

with a ground-state energy difference of about 1.5 eV. Studies of a range of films with different thicknesses, but otherwise prepared under identical deposition conditions, consistently show a strong CT satellite feature for the thickest films (160 nm). Since the amount of structural defects is well known to increase with the film thickness, we attribute the different CT peak intensities to the interaction of Co(3*d*) electrons with donor defect states in the band gap, which are energetically close to and significantly hybridized with these Co(3*d*) states. We also find similar CT peaks in ultrathin (2 nm) Co:TiO_2 films, where the corresponding electronic states most probably involve interfacial species. The hybrid $3d^7$ and $3d^8\underline{L}$ states add to the complex, heterogeneous electronic structure of Co:TiO_2 thin films, and may play a significant role in the rich (magneto-)electronic properties of these materials.

ACKNOWLEDGMENTS

We acknowledge financial support from the NWO-VIDI program (Grants No. 07580 and No. 10246), and the NanoNed program coordinated by the Dutch Ministry of Economic Affairs (Grant No. TMF7155/7156).

[1] T. Dietl, H. Ohno, F. Matsukura, J. Cibert, and D. Ferrand, Science **287**, 1019 (2000).
[2] Y. Matsumoto, M. Murakami, T. Shono, T. Hasegawa, T. Fukumura, M. Kawasaki, P. Ahmet, T. Chikyow, S. Koshihara, and H. Koinuma, Science **291**, 854 (2001).
[3] H. Toyosaki, T. Fukumura, Y. Yamada, K. Nakajima, T. Chikyow, T. Hasegawa, H. Koinuma, and M. Kawasaki, Nat. Mater. **3**, 221 (2004).
[4] S. R. Shinde, S. B. Ogale, J. S. Higgins, H. Zheng, A. J. Millis, V. N. Kulkarni, R. Ramesh, R. L. Greene, and T. Venkatesan, Phys. Rev. Lett. **92**, 166601 (2004).
[5] K. Ueno, T. Fukumura, H. Toyosaki, M. Nakano, and M. Kawasaki, Appl. Phys. Lett. **90**, 072103 (2007).
[6] R. Ramaneti, J. C. Lodder, and R. Jansen, Appl. Phys. Lett. **91**, 012502 (2007).
[7] T. Yamasaki, T. Fukumura, Y. Yamada, M. Nakano, K. Ueno, T. Makino, and M. Kawasaki, Appl. Phys. Lett. **94**, 102515 (2009).
[8] Y. Hirose, T. Hitosugi, Y. Furubayashi, G. Kinoda, K. Inaba, T. Shimada, and T. Hasegawa, Appl. Phys. Lett. **88**, 252508 (2006).
[9] H. Toyosaki, T. Fukumura, K. Ueno, M. Nakano, and M. Kawasaki, Jpn. J. Appl. Phys. Part 2 **44**, L896 (2005).
[10] S. A. Chambers, Surf. Sci. Rep. **61**, 345 (2006).
[11] K. Kikoin and V. Fleurov, Phys. Rev. B **74**, 174407 (2006).
[12] Y. J. Lee, M. P. de Jong, and R. Jansen, Appl. Phys. Lett. **96**, 082506 (2010).
[13] R. Ramaneti, J. C. Lodder, and R. Jansen, Phys. Rev. B **76**, 195207 (2007).
[14] J. Stöhr, *NEXAFS Spectroscopy, Springer Series in Surface Science* Vol. 25 (Springer, Berlin, 1992).
[15] R. D. Cowan, *The Theory of the Atomic Structure and Spectra* (University of California Press, Berkley, 1981); P. H. Butler, *Point Group Symmetry Applications: Methods and Tables* (Plenum, New York, 1981).
[16] H. Ikeno, F. M. F. de Groot, E. Stavitski, and I. Tanaka, J. Phys.: Condens. Matter **21**, 104208 (2009).
[17] F. M. F. de Groot, M. Abbate, J. van Elp, G. A. Sawatzky, Y. J. Ma, C. T. Chen, and F. Sette, J. Phys.: Condens. Matter **5**, 2277 (1993).
[18] F. M. F. de Groot, J. Electron Spectrosc. Relat. Phenom. **67**, 529 (1994).
[19] G. van der Laan, Phys. Rev. B **41**, 12366 (1990).
[20] M. Schuisky, K. Kukli, J. Aarik, J. Lu, and A. Harsta, J. Cryst. Growth **235**, 293 (2002).
[21] R. J. Kennedy and P. A. Stampe, J. Cryst. Growth **252**, 333 (2003).
[22] R. D. Shannon, Acta Crystallogr., Sect. A **32**, 751 (1976).
[23] Y. J. Lee, M. P. de Jong, W. G. van der Wiel, Y. Kim, and J. D. Brock, Appl. Phys. Lett. **97**, 212506 (2010).
[24] A. Lussier, J. Dvorak, Y. U. Idzerda, S. R. Shinde, S. B. Ogale, and T. Venkatesan, Phys. Scr. **T115**, 623 (2005).
[25] X. C. Liu, E. Shi, Z. Z. Chen, T. Zhang, Y. Zhang, B. Y. Chen, W. Huang, X. Liu, L. X. Song, K. J. Zhou, and M. Q. Cui, Appl. Phys. Lett. **92**, 042502 (2008).
[26] F. M. F. de Groot, Chem. Rev. **101**, 1779 (2001).
[27] G. van der Laan, J. Zaanen, G. A. Sawatzky, R. Karnatak, and J.-M. Esteva, Phys. Rev. B **33**, 4253 (1986).
[28] Y. J. Lee, A. Kumar, I. J. Vera Marún, M. P. de Jong, and R. Jansen, IEEE Trans. Magn. **46**, 1683 (2010).